

Single-step microwave mediated synthesis of the  
CoS<sub>2</sub> anode material for high rate hybrid  
supercapacitors†Cite this: *J. Mater. Chem. A*, 2014, 2,  
11099S. Amaresh,<sup>a</sup> K. Karthikeyan,<sup>ab</sup> I.-C. Jang<sup>c</sup> and Y. S. Lee<sup>\*a</sup>

A short time microwave irradiation based synthesis method of phase pure cubic CoS<sub>2</sub> nanoparticles is reported in this study for the first time. The energy density (ED) of hybrid supercapacitors based on CoS<sub>2</sub> as an anode having activated carbon as a cathode has been enhanced by using the higher operating potential of organic electrolytes and by increasing the concentration of the mobile ionic species at the negative electrode, in addition to the lithium ions present in the electrolyte. The specific capacitance delivered by non-lithiated CoS<sub>2</sub> nanoflakes was 52 F g<sup>-1</sup> at a current rate of 0.7 A g<sup>-1</sup> between 0 and 3 V using a LiPF<sub>6</sub>-based electrolyte. Increasing the concentration of the mobile ionic species, *i.e.*, lithium, at the anode enhanced the performance of the hybrid supercapacitor to 119 F g<sup>-1</sup> at a current rate of 0.7 A g<sup>-1</sup>. The hierarchical arrangement of pores in the electroactive material allowed high electrolyte access and reduced the length of the ionic pathway. Consequently, the lithiated form exhibited an ED of 37 W h kg<sup>-1</sup> with a power density of 1 kW kg<sup>-1</sup> at a current rate of 0.7 A g<sup>-1</sup>, compared to only 15 W h kg<sup>-1</sup> for the non-lithiated sample. Furthermore, both samples maintained superior stability over extended cycling for 10 000 cycles at a very high PD of 4 kW kg<sup>-1</sup> with a capacitance retention of 100% for the lithiated sample and 80% for the non-lithiated sample. These results will be useful in the fabrication of high ED, high rate hybrid supercapacitors for electric vehicle applications.

Received 4th April 2014

Accepted 1st May 2014

DOI: 10.1039/c4ta01633e

www.rsc.org/MaterialsA

## Introduction

The power performance gap between batteries and capacitors in a Ragone plot was bridged by the discovery and industrial introduction of the promising energy storage devices known as supercapacitors, which offer high power density (PD), high energy density (ED) compared to conventional capacitors, long service life, highly dynamic charge propagation and simple operating principle.<sup>1,2</sup> Apart from time-dependent consumer electronic devices, supercapacitors are expected to be integrated into electric vehicle applications, in which the energy released during braking can be recovered by the ultrafast charge-discharge process of supercapacitors. Hybrid supercapacitors have recently gained interest owing to their increased ED, aside from their high PD. Unlike lithium ion capacitors (LICs) that use carbonaceous materials as electrodes, hybrid supercapacitors consist of an electrical double layer forming active

material, such as activated carbon, as the positive electrode and a battery-type electrode material as the negative electrode. In this conjunction, the charge storage mechanism is established through a reversible non-faradic reaction, using anions, at the surface of the positive electrode and a faradic reaction at the negative electrode side. Two methods are used to improve the ED of capacitors according to the formula  $ED = (1/2)CV^2$ , where  $C$  is the capacitance and  $V$  is the voltage: (i) introducing the pseudo capacitive effect in electrochemical capacitors and (ii) operating the supercapacitors in a high potential range with the help of organic electrolytes that are capable of withstanding higher voltages, *i.e.*, >3 V. Traditionally RuO<sub>2</sub>, MnO<sub>2</sub>, Ni(OH)<sub>2</sub>, Co<sub>3</sub>O<sub>4</sub>, Fe<sub>3</sub>O<sub>4</sub>, SnO<sub>2</sub>, and TiO<sub>2</sub> were used as pseudocapacitive electrode materials for hybrid supercapacitors and have been extensively studied.<sup>3–8</sup> Additionally, materials including Ni(OH)<sub>2</sub>, Co(OH)<sub>2</sub>, Nb<sub>2</sub>O<sub>5</sub>, V<sub>2</sub>O<sub>5</sub>, TiP<sub>2</sub>O<sub>7</sub> and Li<sub>2</sub>CoPO<sub>4</sub>F have also shown pseudocapacitive behaviour.<sup>9–13</sup> Most of these materials showed higher ED than conventional double layer capacitors, thus decreasing the gap between batteries and capacitors.

Despite this extensive research focus, electrochemical capacitors still suffer from limited ED when compared with conventional batteries, especially Li-ion batteries where Li ion is reversibly intercalated in the electrode material, thereby increasing the ED significantly while the PD is being improved to meet traditional capacitors. Unfortunately, electrolyte

<sup>a</sup>Faculty of Applied Chemical Engineering, Chonnam National University, Gwang-ju 500-757, Korea. E-mail: leey@chonnam.ac.kr; Tel: +82 62 530 1904

<sup>b</sup>Department of Mechanical and Materials Engineering, The University of Western Ontario, London, Ontario, N6A 5B9, Canada

<sup>c</sup>Department of Applied Chemistry, Faculty of Engineering, Kyushu University, 744 Motoooka, Fukuoka 819-0395, Japan

† Electronic supplementary information (ESI) available. See DOI: 10.1039/c4ta01633e

decomposition above a certain threshold has limited the increase of the voltage range. Hence, improving the capacitance of electrode materials has focused more on adopting strategies such as improving symmetric capacitors using pseudocapacitive electrode materials, changing the porous structure of carbon and developing asymmetric capacitors with electrodes made of different materials.<sup>14–16</sup> Electrochemical capacitors using organic electrolytes containing lithium salts dissolved within operate on the reversible reaction of Li ions sourced from the electrolyte along with the anion surface adsorption-desorption phenomena as the charge-storage mechanism. This decreases the concentration of the lithium salt in the electrolyte due to the partial reversibility of ionic species during operation and lowers the conductivity of the electrolyte. For example, in the case of Li-ion capacitors, the initial charge-discharge cycle uses Li ions present in the cell for stable solid-electrolyte interphase (SEI) layer formation. Most of these Li ions are obtained from the electrolyte, thereby decreasing the overall Li concentration in the electrolyte and reducing the long-term cycleability.<sup>16</sup> One possible approach adopted to overcome this issue is to pre-lithiate the negative electrode using a sacrificial metal electrode prior to capacitor fabrication.<sup>17–19</sup> The pre-lithiated electrode allows low consumption of Li ions from the electrolyte, although the anions present in the electrolyte continue to participate in the formation of the SEI layer. The electrolyte conductivity is maintained throughout the cycling, which enhances the performance. An improved cycle life, enhanced ED, reduced electrode resistance and reduced irreversibility of negative electrode are the positive outcomes obtained by adopting the pre-doping procedure.<sup>18</sup> Conversion-type electrode active materials, which are capable of forming lithium-based by-products during the faradic reaction, can be pre-lithiated to achieve the same advantages. This mechanism is advantageous in the process of developing hybrid supercapacitors, which are designated to have a higher ED than their capacitor counterparts.

Elemental sulfur is considered a promising electrode material for high ED batteries, because the theoretical capacity of sulfur is  $1672 \text{ mA h g}^{-1}$  which transforms into a theoretical specific ED of  $2500 \text{ W h kg}^{-1}$ .<sup>20</sup> Nevertheless, sulfur suffers from low electronic conductivity, formation of polysulfides with electrolyte components and noticeable volume expansion and contraction during electrochemical reactions. On the other hand, the lithiated form of sulfur, *i.e.*,  $\text{Li}_2\text{S}$ , has attracted interest with an inherent theoretical specific capacity ( $C_{\text{sp}}$ ) of  $1166 \text{ mA h g}^{-1}$ .<sup>20</sup> Transition metal sulfides such as  $\text{FeS}_2$ ,  $\text{CuS}$ ,  $\text{CoS}_2$ ,  $\text{CoS}$ ,  $\text{Co}_9\text{S}_8$ , and  $\text{SnS}_2$  have been explored for battery applications, but have been less investigated for supercapacitor applications that specifically involve lithium ions as the mobile ionic species, even though elemental sulfur shares the same group as that of the oxide in the periodic table and is expected to have similar properties to those of the oxide analogues.<sup>21–27</sup> In contrast, metal sulfides have been widely explored for non-Li ion based supercapacitor applications, for example  $\text{CoS}_2$ ,<sup>28</sup>  $\text{Ni}_3\text{S}_2$  (ref. 29) and  $\text{Ni}_x\text{Co}_{3-x}\text{S}_4$ .<sup>30</sup> Cobalt sulfides have been applied in various fields such as semiconductors, catalysis, and magnetic materials due to their inherent higher electronic

properties that can be utilized for higher rate performance in the case of batteries. Cobalt disulfide ( $\text{CoS}_2$ ) has a higher thermal stability than  $\text{FeS}_2$ .<sup>21,23,25,27</sup> On this basis,  $\text{CoS}_2$  with a Gibbs free energy of  $-146 \text{ kJ mol}^{-1}$  was selected for evaluating the capacitance behaviour against an activated carbon positive electrode for hybrid supercapacitor applications. The negative Gibbs free energy of  $\text{CoS}_2$  signified a highly spontaneous thermodynamically feasible reduction reaction. This type of hybrid configuration having a battery type electrode and an electric double layer type electrode in the presence of a Li-ion conducting electrolyte can also be called as a Li-ion capacitor. Previous reports suggested an expensive synthesis methodology based on a high pressure hydrothermal process, which requires heavy autoclaves and a long duration for synthesis.<sup>21,25,27,31–34</sup> In this study, therefore, nano-crystalline  $\text{CoS}_2$  flakes were synthesized based on an inexpensive raw material, namely thiourea, through a solution-based, single-step, quick microwave irradiation technique. Consequently, the heat treatment step was reduced and thus can be easily adopted in the industry. In the absence of any published report on the use of  $\text{CoS}_2$  in hybrid supercapacitor applications with a high voltage window of the 0–3 V range, the synthesized  $\text{CoS}_2$  active materials were subjected to rigorous high rate testing in a  $\text{LiPF}_6$ -based organic electrolyte. The obtained powders were further lithiated to increase the specific ED and evaluated in a hybrid supercapacitor arrangement at various high current rates. The lithiation doubled the ED of the hybrid supercapacitor compared to that of the corresponding undoped form.

## Experimental section

The starting materials, thiourea (99%, Sigma Aldrich) and cobalt(II) chloride hexahydrate (99%, Wako) were used as received without any further purification. In a typical synthesis, 15 mmol salt of cobalt was dissolved in 50 ml deionized water under vigorous stirring at  $50^\circ\text{C}$  for 20 min. About 80 mmol thiourea was then added to this solution and the mixture was further maintained at  $50^\circ\text{C}$  for 30 min under stirring before being irradiated. The mixture was then carefully transferred to a household microwave oven and exposed to microwave irradiation with a power of 700 W for 20 min. The resultant product was allowed to cool down to room temperature naturally, washed with water and ethanol several times to remove the residuals and finally dried at  $60^\circ\text{C}$  overnight. The as-synthesized nanoflakes of  $\text{CoS}_2$  were used for physical and electrochemical characterizations without any further heat treatment.

The phase constituents of the  $\text{CoS}_2$  nanoflakes were confirmed by using an X-ray powder diffractometer (XRD, Rint 1000, with  $\text{CuK}\alpha$  radiation  $\lambda = 1.5406 \text{ \AA}$ ). The morphological characteristics were observed using a field emission scanning electron microscope (FESEM, S-4700, Hitachi) and a transmission electron microscope (TEM, TECNAI, Philips) operated at 200 keV. The surface area and the nitrogen absorption-desorption isotherm were analyzed using an ASAP 2020 (Micromeritics) analyzer. X-ray photoelectron spectroscopy (XPS, Multilab2000, VG) was used to analyze the composition of the prepared samples. The measurement was carried out under

ultra high vacuum and the spectrometer was calibrated using the C 1s line of the 285.0 eV binding energy of graphitic carbon. Electrochemical impedance spectroscopy (EIS) and cyclic voltammetry (CV) studies were performed using an electrochemical work station (SP-150, Biologic) at room temperature on freshly prepared cells. A battery cycler (WBCS 3000, Won-A-Tech, Korea) was used for the charge–discharge studies.

Electrochemical studies were carried out in a coin-type CR2032 cell assembled in an argon-filled glove box. Briefly, the cell electrodes were prepared by coating a slurry containing 70% active material, 15% conductive additive (Ketjen black) and 15% binder (Teflonized acetylene black) over a stainless steel mesh. The electrodes were then dried at 160 °C for 4 h in a vacuum before the cell was assembled in the argon-filled glove box. Activated carbon was used as the cathode and CoS<sub>2</sub> nanoflakes served as the anode for the hybrid supercapacitors constructed with 1 M LiPF<sub>6</sub> dissolved in EC–DMC (1 : 1, v/v) as an electrolyte. An anode to cathode mass ratio of 1 : 3 was maintained throughout the study and the optimization process is described in the ESI.† CV and charge–discharge studies were carried out between 0 and 3 V, while the impedance spectra were recorded in the frequency range of 100 kHz to 100 mHz.

## Results and discussion

Crystalline nanoflakes of cattierite CoS<sub>2</sub> with a cubic phase were synthesized by simple, single-step microwave synthesis. The absence of any reflections of co-existent phases such as CoS, Co<sub>3</sub>S<sub>4</sub> and Co<sub>9</sub>S<sub>8</sub> in the XRD data confirmed the preparation of phase-pure CoS<sub>2</sub> nanoflakes with the reflection of the *Pa*3(205) space group. The lattice constant ( $a = 5.54$  Å) and XRD patterns

in Fig. 1a matched well with those reported in JCPDS card 41-1471 and previous studies.<sup>21,31–34</sup> Various researchers have encountered complexity in formulating phase-pure CoS<sub>2</sub>. For example, preparation of cobalt sulfide in a redox atmosphere using toluene involving Zn or I<sub>2</sub> as the catalyst has resulted in multiple phases, such as Co<sub>3</sub>S<sub>4</sub>, CoS<sub>2</sub>, and Co<sub>9</sub>S<sub>8</sub>, depending upon the temperature.<sup>24</sup> Wang *et al.* reported mixed phases of cobalt sulfides such as CoS<sub>2</sub>, Co<sub>9</sub>S<sub>8</sub> and CoS during synthesis.<sup>22</sup> In the current study, phase-pure CoS<sub>2</sub> was prepared in a reduction atmosphere using thiourea as both the sulfur source and the reducing agent. The microwave route enabled rapid synthesis of nanocrystals, which largely inhibited particle growth and also reduced the additional heat treatment step involved in a solvent-based synthesis methodology.<sup>35</sup> The *in situ* heat developed during the breaking down of thiourea resulted in a carbon cloud over the CoS<sub>2</sub> nanoflakes that enhanced the electronic conductivity and the electrochemical properties. XPS results (Fig. S5†) revealed the formation of CoS<sub>2</sub> in the presence of Co 2P<sub>3/2</sub> and Co 2P<sub>1/2</sub> peaks at 780.4 eV and 796.1 eV, respectively, while the S 2p<sub>3/2</sub> peak was found at 163.7 eV.

The nitrogen adsorption–desorption isotherm and the pore size distribution curves (Fig. 1b) suggested the formation of mesopores and macropores and can therefore be used to elucidate the pore structure developed during the microwave heating process. The absence of a steep rise in the nitrogen isotherm at relative pressure near to 0.01 revealed the absence of any micropores in the synthesized material, while the capillary condensation step representing the hysteresis loop and the isotherm behaviour after  $P/P_0 = 0.9$  indicated the development of mesoporosity and macroporosity, respectively. The pores were mainly distributed within the range of 2–50 nm, known as mesopores, with few pores in the macropore region having a maximum size of 185 nm. The macropores help in the formation of ion reservoirs to reduce the diffusion distance to the interior surface and the mesopore walls supply a less resistant ionic pathway for ions to reach the interior of the particles providing maximum coverage for CoS<sub>2</sub> nanoflakes.<sup>36,37</sup> This categorical arrangement of pores can offer good capacitive behaviour through rapid ionic transportation and a short ion diffusion path. Thus, CoS<sub>2</sub> nanoflakes submerged in a carbon cloud are expected to exhibit a superior capacitive activity along with a stable cycle life.

Surface morphological studies revealed the formation of CoS<sub>2</sub> nanoflakes and a carbon cloud over the crystals, as shown in Fig. 2a. The SEM images clearly show the cluster formation of CoS<sub>2</sub> nanoflakes to a size of one micrometer. The formation of intermediate pores was easily visible on the surface of the agglomerated particles. These pores enhanced the specific surface area, increased the accessibility of the electrolyte and thereby provided more sites for the adsorption/desorption process. This in turn can be augmented for obtaining higher  $C_{sp}$  and increased cycle stability. In addition, the formation of a highly porous carbon cloud can be seen in the low resolution TEM pictures dominated by a dark region with CoS<sub>2</sub> nanoflakes of size ~10 nm seen distributed uniformly over the entire carbon cloud. The agglomerated nanoflakes were randomly oriented, as seen from the high resolution TEM image (Fig. 2b).

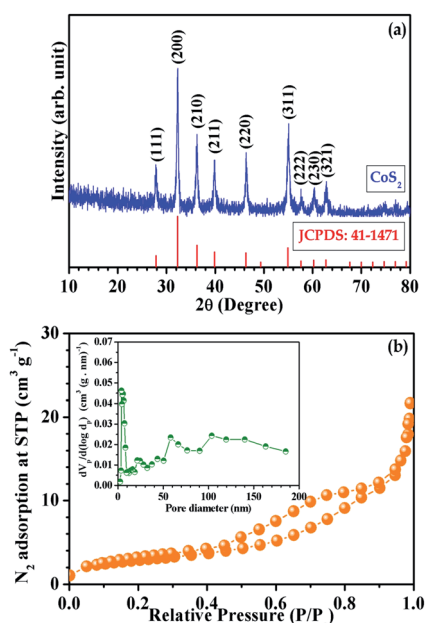


Fig. 1 (a) XRD pattern of the single-step microwave synthesized CoS<sub>2</sub> nanoflakes and (b) N<sub>2</sub> adsorption–desorption curves of the as-synthesized CoS<sub>2</sub> sample with the pore size distribution given in the inset.



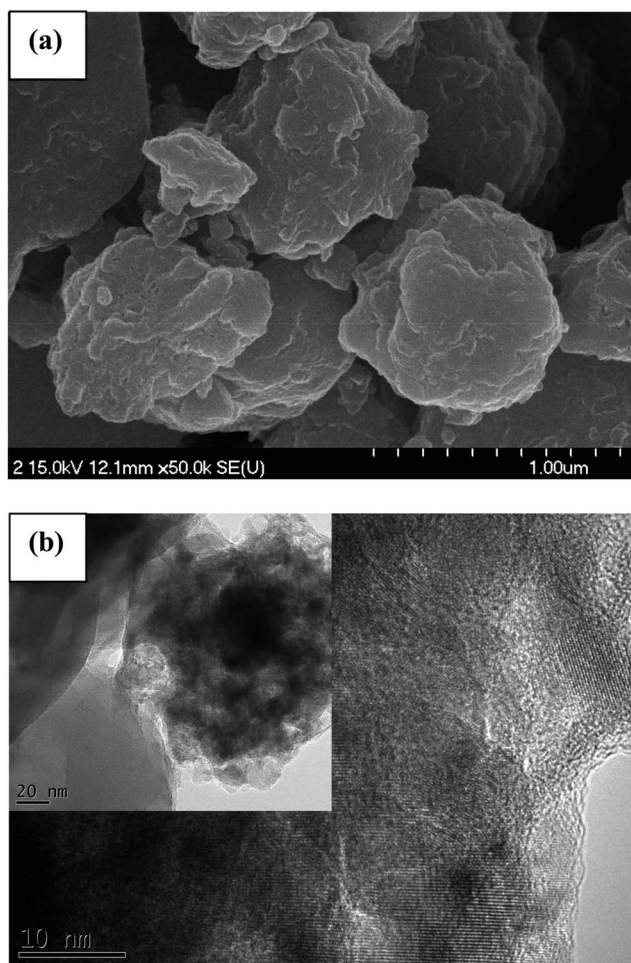


Fig. 2 (a) SEM image of the as-synthesized  $\text{CoS}_2$  sample, and (b) low and high magnification TEM images of the non-lithiated  $\text{CoS}_2$  sample.

The porous network thus created can increase the electrolyte uptake and increase the electrochemical area for pseudocapacitance. A comprehensible investigation of the pores using nitrogen adsorption has supported the pore distribution thus described.

LICs are capable of delivering a higher ED compared with conventional electrochemical double layer capacitors. To further increase the ED of LICs, lithium doping at the anode has been carried out using metallic lithium or compounds containing lithium.<sup>12–14,16</sup> The hybrid supercapacitor investigated in this study, based on an activated carbon cathode and a  $\text{CoS}_2$  anode, can be doped with lithium at the anode side for ED enhancement. Electrochemical lithiation can be used to control lithium doping, thereby increasing the total amount of lithium participation in the electrochemical charge storage. Furthermore, electrochemical lithiation can also induce nanoporous particle formation that enhances the overall surface area and reduces the inter-particle distance for lithium ion displacement.<sup>38</sup> The electrochemical process followed during the lithiation of  $\text{CoS}_2$  was  $4\text{Li} + \text{CoS}_2 \rightarrow \text{Co} + 2\text{Li}_2\text{S}$ . A fresh half cell containing  $\text{CoS}_2$  as the anode against a lithium metal cathode was constructed and then electrochemical lithiation was carried

out at  $1.0 \text{ A g}^{-1}$ . The lithiation process (Fig. S1†) exhibited the typical behaviour of a conversion-type negatively active material with a voltage plateau at  $\sim 1.4 \text{ V}$ , despite the very high current of the reaction. The metallic cobalt thus formed during the reaction acted as a catalyst during further electrochemical studies.<sup>20,39</sup> The as-prepared or non-lithiated  $\text{CoS}_2$  nanoflakes ( $\text{NL-CoS}_2$ ) and the corresponding lithiated form ( $\text{L-CoS}_2$ ) were simultaneously tested for hybrid supercapacitor applications and the results are discussed in detail.

CV studies were carried out to check the capacitive function and stability of the as-prepared and lithiated electrodes at various scan rates. The results reported in Fig. 3a clearly highlighted the capacitive properties of both electrodes with the formation of a typical rectangular shaped current response with respect to voltage.  $C_{\text{sp}}$  was calculated from CV traces using the following formula:  $C_{\text{sp}} = I/(\text{mass} \times R)$ , where  $R$  is the scan rate during measurement and  $I$  is the current response obtained. The CV traces were recorded at a scan rate of  $10 \text{ mV s}^{-1}$  and the calculated  $C_{\text{sp}}$  was 36 and  $74 \text{ F g}^{-1}$  for  $\text{NL-CoS}_2$ - and  $\text{L-CoS}_2$ -containing cells, respectively. The CV traces recorded at various other scan rates showed capacitive behaviour from scan rates as low as  $5 \text{ mV s}^{-1}$  to  $50 \text{ mV s}^{-1}$ , as shown in Fig. S2.† The current response increased with increasing scan rates for both materials and maintained the rectangular shape, which revealed the highly reversible characteristics of both materials. There was a noticeable increase in the current response of  $\text{L-CoS}_2$ , as it responded with twice the current at all scan rates compared to the non-lithiated sample. The superior response was attributed to the nano-porous structure formation during the lithiation process that allowed electrolyte accessibility and high ionic mobility during the electrochemical reaction. The reaction mechanism was attributed to the reversible intercalation of Li ions from the electrolyte at the anode and the formation of electrical double layer charge storage at the AC cathode. In the case of the lithiated  $\text{CoS}_2$  sample, the additional lithium ions from the anode participated in the charge storage process, thus increasing the overall electrochemical activity of the hybrid supercapacitor. The additional lithium ions were believed to be involved in the reversible intercalation process, while the lithium ions in the electrolyte were reversibly adsorbed on the electrode surface, which increased the ED of the hybrid supercapacitor. Consequently, the loss of lithium in the electrolyte was avoided and the cell stability was enhanced.

This mechanism was further confirmed by charge–discharge studies over a range of high current rates from  $0.7 \text{ A g}^{-1}$  to  $2.7 \text{ A g}^{-1}$ . The mass ratio for asymmetric capacitors was optimized based on the half cell charge–discharge characteristics, as shown in Fig. S3.† Accordingly, the operating potential for the  $\text{CoS}_2/\text{AC}$  hybrid capacitors was set at 0–3 V, which is well suited to safe operation without electrolyte decomposition. The chrono-potentiometric curves of the AC cathode with the metal sulfide anodes in 1 M  $\text{LiPF}_6$  dissolved in the EC–DMC (1 : 1 v/v) electrolyte obtained at  $0.7 \text{ A g}^{-1}$  are shown in Fig. 3b. The symmetrical triangular-shaped curves for the cells containing both  $\text{NL-CoS}_2$  and  $\text{L-CoS}_2$  represented the standard behaviour of capacitors with a calculated coulombic efficiency of 94% for  $\text{NL-CoS}_2$  and >99% for  $\text{L-CoS}_2$  samples during the first cycle. The

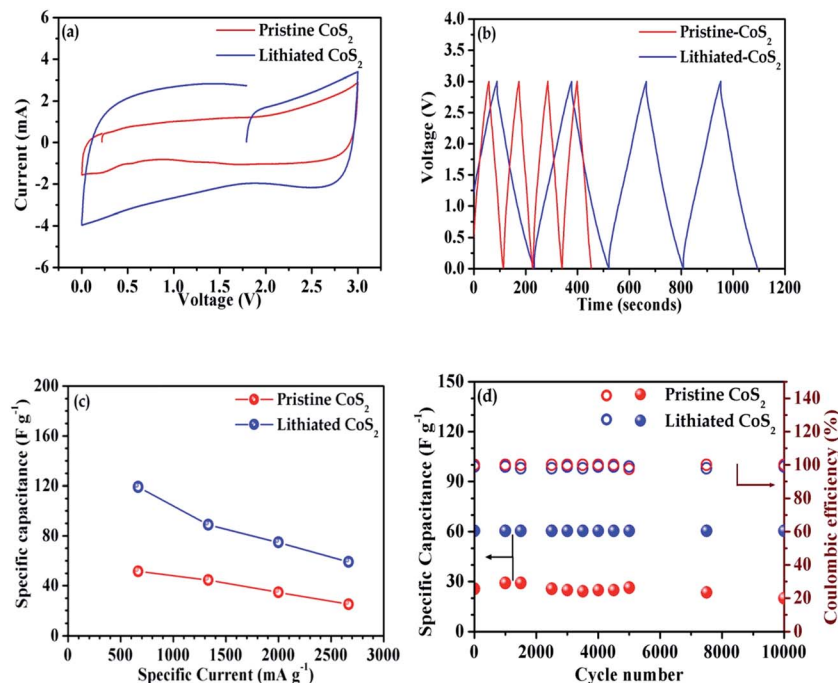


Fig. 3 Electrochemical characteristics of the non-lithiated and lithiated  $\text{CoS}_2$  samples: (a) cyclic voltammogram at  $10 \text{ mV s}^{-1}$ , (b) charge-discharge curves at  $0.7 \text{ A g}^{-1}$ , (c) variation of specific capacitance ( $C_{\text{sp}}$ ) with current and (d) long-term cycling at a high current rate of  $2.7 \text{ A g}^{-1}$  (open circles represent the Coulombic efficiency and closed circles signify  $C_{\text{sp}}$ ).

asymmetric cells exhibited well defined symmetrical curves at all current rates, including a sudden  $IR$  drop or increase during the discharge or charge process, respectively. The equivalent series resistance was responsible for the  $IR$  drop in the capacitors, which includes the electrolyte resistance, electrode resistance and contact resistance between the electrode and the electrolyte.<sup>40</sup> The formation of highly networked  $\text{Li}_2\text{S}$  and  $\text{Co}$  during lithiation reduced the inter-particle distance and thus increased the conductivity of the lithiated sample, thereby decreasing the  $IR$  drop during the charge-discharge studies, as compared with the NL- $\text{CoS}_2$  sample, in addition to the positive effect of the highly efficient cobalt catalyst during the supercapacitor operation.

The  $C_{\text{sp}}$  values were calculated from the charge-discharge curves using the formula  $C_{\text{sp}} = 4(It/mV)$ ,<sup>41</sup> where  $I$  is the current applied within the voltage range ( $V$ ),  $t$  the time for the cell to respond to the applied current and  $m$  the total mass of the active materials used in both electrodes. The capacitance delivered by the hybrid supercapacitor at a rate of  $0.7 \text{ A g}^{-1}$  was  $52 \text{ F g}^{-1}$  for NL- $\text{CoS}_2/\text{AC}$  and  $119 \text{ F g}^{-1}$  for L- $\text{CoS}_2/\text{AC}$  cells within the potential region of  $0-3 \text{ V}$ . When tested at different current densities (Fig. 3c), the cells retained  $44$ ,  $35$  and  $25 \text{ F g}^{-1}$  for NL- $\text{CoS}_2/\text{AC}$  and  $89$ ,  $75$  and  $60 \text{ F g}^{-1}$  for L- $\text{CoS}_2/\text{AC}$  at current rates of  $1.3$ ,  $2.0$  and  $2.7 \text{ A g}^{-1}$ , respectively. The  $C_{\text{sp}}$  of the lithiated form was more than twice that of the non-lithiated sample at all current densities with an appreciable increase in rate capability. The increase in  $C_{\text{sp}}$  for the L- $\text{CoS}_2$  sample was ascribed to the presence of additional movable lithium ions in the electrode, the increase in conductivity and the decrease in inter-particle distance due to the high accessibility for the electrolyte. The

$\text{CoS}_2/\text{AC}$  cell used the lithium ions from the electrolyte during the charge-discharge process because of the lack of lithium at the electrodes for the conversion reaction at the anode side. This mechanism resulted in lithium depletion at the electrolyte and ultimately reduced the  $C_{\text{sp}}$  during cycling. Furthermore, the reversible formation of  $\text{CoS}_2$  at the L- $\text{CoS}_2$  cell acted to increase the ED of the hybrid supercapacitor cell. The alternative method of doping the graphitic electrode with metallic lithium for enhancing ED is potentially dangerous because lithium metal is highly reactive and can cause undesired side reactions with the release of enormous heat when not properly handled. Instead, the formation of thermodynamically stable products such as  $\text{Li}_2\text{S}$  can be effective in increasing the ED of electrochemical capacitors. On the other hand, the decrease in capacitance for both cells with increasing current rate can be attributed to the reduced participation of active materials at the ultra high rate currents.<sup>42</sup>

The application of hybrid supercapacitors in electric vehicles for regenerating energy during braking will necessitate long-term electrochemical performance and a high current test for assessing the threshold limit of the material. To further confirm the cyclability of the  $\text{CoS}_2/\text{AC}$  hybrid supercapacitors, a high current rate cycling study at  $2.7 \text{ A g}^{-1}$  was carried out and the results are presented in Fig. 3d and S4.† Stable cycling was observed for the L- $\text{CoS}_2/\text{AC}$  cell which maintained a  $C_{\text{sp}}$  of  $\sim 60 \text{ F g}^{-1}$ , while the NL- $\text{CoS}_2/\text{AC}$  cell exhibited variable cycling with a maximum  $C_{\text{sp}}$  of  $29 \text{ F g}^{-1}$  after 1000 cycles and then maintained stable cycling up to 5000 cycles at  $25 \text{ F g}^{-1}$ . The cycle stability of the NL- $\text{CoS}_2/\text{AC}$  cell decreased after 5000 cycles and the  $C_{\text{sp}}$  reached  $\sim 20 \text{ F g}^{-1}$  after 10 000 cycles at  $2.7 \text{ A g}^{-1}$ . The

capacitance decrease of the CoS<sub>2</sub>/AC cell was attributed to the reduced coulombic efficiency after 5000 cycles. The decreased number of lithium ions in the electrolyte reduced the capacitance to about 80% of that observed at the initial cycles. The depletion in lithium ions in the electrolyte was avoided in the lithiated CoS<sub>2</sub> sample, resulting in the excellent capacitance of the L-CoS<sub>2</sub>/AC cell, twice that of the non-lithiated sample, with stable capacitance retention and a coulombic efficiency of 100% up to 10 000 cycles. The microwave synthesis of CoS<sub>2</sub> nanoflakes resulted in the formation of nanometer-scale particles. Furthermore, the particle formation during lithiation reduced the inter-particle distance, which increased the overall area of active materials and thus contributed to the superior electrochemical performance of the lithiated CoS<sub>2</sub> sample. Nanostructured materials having high surface area, high surface energy and activity, and high porosity can be used to establish new active sites for reactions, reduce the specific surface current rate, decrease the length of the lithium ion pathway and thus improve the specific ED and cycle stability.

The Ragone plot representing the ED and PD obtained for the synthesized CoS<sub>2</sub> nanoflakes and the corresponding lithiated form was calculated from charge–discharge studies using the formula provided in the ESI.† Fig. 4 clearly shows the definite two-fold increase in the ED of the lithiated form compared with that of the non-lithiated CoS<sub>2</sub> sample and also definitely higher than some of the capacitors. For example, the EDs exhibited by the NL-CoS<sub>2</sub> and L-CoS<sub>2</sub> samples were 15 and 37 W h kg<sup>−1</sup>, respectively, with a PD of 1 kW kg<sup>−1</sup> at a current rate of 0.7 A g<sup>−1</sup>. At the highest current rate of 2.7 A g<sup>−1</sup>, the delivered ED was 9 W h kg<sup>−1</sup> for non-lithiated and 19 W h kg<sup>−1</sup> for the lithiated sample with a PD of 4 kW kg<sup>−1</sup>. Thus, the ED can be increased by lithiating the conversion-type electroactive materials and by increasing the operating voltage by using a suitable electrolyte and mass ratio in the electrode. The ED obtained for L-CoS<sub>2</sub> in this study (37 W h kg<sup>−1</sup>) at a PD of 1 kW kg<sup>−1</sup> was higher than that of hierarchical porous graphitic carbon (20 W h kg<sup>−1</sup>),<sup>37</sup> mesoporous carbon (19 W h kg<sup>−1</sup>),<sup>43</sup> mesoporous carbon-rGO composite (18 W h kg<sup>−1</sup>),<sup>44</sup> MnO<sub>2</sub> nanosheets (<30 W h kg<sup>−1</sup>),<sup>45</sup> conducting polymer hybrid supercapacitors (22 W h kg<sup>−1</sup>)<sup>46</sup> and graphene-MnO<sub>2</sub> nanoplates (23 W h kg<sup>−1</sup>).<sup>47</sup> Most of the active materials for these high rate supercapacitors

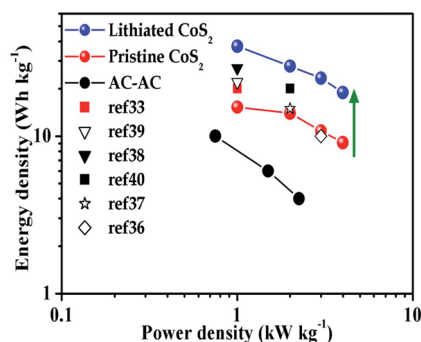


Fig. 4 Ragone plot of hybrid supercapacitor cells containing non-lithiated and lithiated CoS<sub>2</sub> samples including the comparison from various other studies.

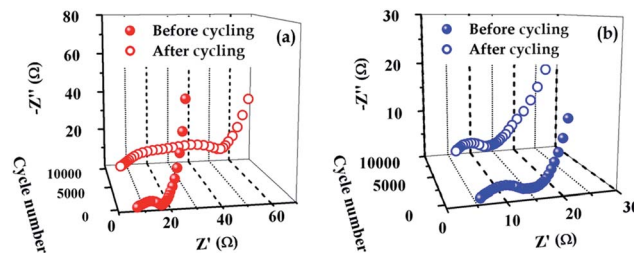


Fig. 5 Electrochemical impedance plots of pristine (a) and lithiated (b) samples before and after 10 000 cycles at a current rate of 2.7 A g<sup>−1</sup>.

were tuned for maximizing the porosity in order to increase the electroactive area, but at the expense of decreased PD. On the other hand, the ED of supercapacitors has to be optimized by combining different strategies, *i.e.*, increasing the  $C_{sp}$  by improving the area, operating the capacitors at a higher potential window for gaining additional ED without deferring the PD and introducing additional mobile ions in the electrode that are responsible for capacitance to avoid the electrolyte depletion issue. Further, the conversion-type anodes recovered from used battery cells can be used in a supercapacitor configuration for additional cycling. Thus the recycling of active materials can be achieved, leading to decreased environmental concerns.

EIS is an important tool for accessing the performance of an active material for supercapacitor applications as it directly quantifies the extent of resistance involved in the cell. The Nyquist plots of the NL-CoS<sub>2</sub> and L-CoS<sub>2</sub> active materials before and after 10 000 cycles at 2.7 A g<sup>−1</sup> are presented in Fig. 5. All the plots had two semicircles in the high to medium frequency region and a sloping line representing the diffusion control process in the low frequency region. The intercepts of each semicircle to the real axis can be interpreted for a faradic charge transfer resistance at the AC electrode and ionic charge transfer resistance at the anode, while the high frequency intercept to the real axis was attributed to the solution resistance developed from the electrolyte. The overall charge transfer resistance for the L-CoS<sub>2</sub> sample remained at the initial ~9 Ω, even after 10 000 cycles, which indicated the non-depletion of lithium ions at the electrolyte and hence led to superior cycle stability and coulombic efficiency. In the case of NL-CoS<sub>2</sub>, the resistance increased from initial 9 Ω to ~50 Ω after 10 000 cycles. The ionic charge transfer resistance contributed a maximum resistance of 35 Ω to the overall resistance, which clearly demonstrated the decreased lithium ion mobility during high rate cycling. Future studies can be directed at achieving higher ED by further increasing the voltage with the ability of the variable operating potential of diverse battery-type materials available as an electrode active material in hybrid supercapacitor configuration.

## Conclusion

Single phase CoS<sub>2</sub> was prepared using inexpensive starting materials with a short microwave irradiation procedure, while avoiding the complexity involved in the highly prevalent hydrothermal route. The porosity developed during this quick



preparation method helped to retain high  $C_{sp}$  for  $\text{CoS}_2$  materials in the 0–3 V range. The ED of the materials was further increased by lithiating the conversion-type negative active material prior to the fabrication of the hybrid supercapacitors. The reaction mechanism in the lithiated form essentially followed the same concept, except for the reversed direction of the reaction, which promoted more of the mobile ionic species, *i.e.*, lithium. The increased surface area, decreased inter-particle distance, improved ionic conductivity, and reduced *IR* drop were the factors that helped improve the electrochemical activity of the lithiated  $\text{CoS}_2$  nanoflakes. The cycle stability of the lithiated sample was governed by the unrelenting resistance maintained at an ultra high current rate and the non-depletion of lithium ions in the electrolyte. The depletion of lithium ions in the electrolyte was held responsible for the reduced capacitance and the cycle stability of the non-lithiated sample.

## Acknowledgements

This research was supported by the Basic Science Research Program through the National Research Foundation of Korea (NRF) funded by the Ministry of Education (NRF-2009-0094055).

## References

- 1 P. Simon and Y. Gogotsi, *Nat. Mater.*, 2008, **7**, 845–854.
- 2 P. J. Hall, M. Mirzaei, S. I. Fletcher, F. B. Sillars, A. J. R. Rennie, G. O. Shitta-Bey, G. Wilson, A. Cruden and R. Carter, *Energy Environ. Sci.*, 2010, **3**, 1238–1251.
- 3 K. Karthikeyan, S. Amaresh, D. Kalpana, R. K. Selvan and Y. S. Lee, *J. Phys. Chem. Solids*, 2012, **73**, 363–367.
- 4 H. Jiang, C. Z. Li, T. Sun and J. Ma, *Nanoscale*, 2012, **4**, 807–812.
- 5 R. Vellacheri, V. K. Pillai and S. Kurungot, *Nanoscale*, 2012, **4**, 890–896.
- 6 S. Liu, S. H. Sun and X. Z. You, *Nanoscale*, 2014, **6**, 2037–2045.
- 7 S. Chen, W. Xing, J. J. Duan, X. J. Hu and S. Z. Qiao, *J. Mater. Chem. A*, 2013, **1**, 2941–2954.
- 8 K. Karthikeyan, D. Kalpana, S. Amaresh and Y. S. Lee, *RSC Adv.*, 2012, **2**, 12322–12328.
- 9 G. J. Park, D. Kalpana, A. K. Thapa, H. Nakamura, Y. S. Lee and M. Yoshio, *Bull. Korean Chem. Soc.*, 2009, **30**, 817–820.
- 10 K. Karthikeyan, S. Amaresh, K. J. Kim, S. H. Kim, K. Y. Chung, B. W. Cho and Y. S. Lee, *Nanoscale*, 2013, **5**, 5958–5964.
- 11 G. W. Yang, C. L. Xu and H. L. Li, *Chem. Commun.*, 2008, 6537–6539.
- 12 V. Aravindan, M. V. Reddy, S. Madhavi, S. G. Mhaisalkar, G. V. S. Rao and B. V. R. Chowdari, *J. Power Sources*, 2011, **196**, 8850–8854.
- 13 P. K. Nayak and N. Munichandraiah, *J. Electrochem. Soc.*, 2008, **155**, A855–A861.
- 14 A. Burke, *J. Power Sources*, 2000, **91**, 37–50.
- 15 W. G. Pell and B. E. Conway, *J. Power Sources*, 2004, **136**, 334–345.
- 16 B. E. Conway, *Electrochemical supercapacitors: scientific fundamentals and technological applications*, Plenum Press, New York, 1999.
- 17 S. R. Sivakkumar and A. G. Pandolfo, *Electrochim. Acta*, 2012, **65**, 280–287.
- 18 M. S. Park, Y. G. Lim, J. H. Kim, Y. J. Kim, J. Cho and J. S. Kim, *Adv. Energy Mater.*, 2011, **1**, 1002–1006.
- 19 T. Aida, K. Yamada and M. Morita, *Electrochem. Solid-State Lett.*, 2006, **9**, A534–A536.
- 20 X. L. Ji and L. F. Nazar, *J. Mater. Chem.*, 2010, **20**, 9821–9826.
- 21 J. M. Yan, H. Z. Huang, J. Zhang, Z. J. Liu and Y. Yang, *J. Power Sources*, 2005, **146**, 264–269.
- 22 P. F. Yin, L. L. Sun, Y. L. Gao and S. Y. Wang, *Bull. Mater. Sci.*, 2008, **31**, 593–596.
- 23 R. A. Guidotti and P. Masset, *J. Power Sources*, 2006, **161**, 1443–1449.
- 24 X. F. Qian, X. M. Zhang, C. Wang, Y. Xie and Y. T. Qian, *Inorg. Chem.*, 1999, **38**, 2621–2623.
- 25 B. Liu, F. F. Wang, D. F. Zheng, X. C. Liu, X. J. Sun, S. Y. Hou and Y. Xing, *Mater. Lett.*, 2011, **65**, 2804–2807.
- 26 Z. F. Jiang, C. Wang, G. H. Du, Y. J. Zhong and J. Z. Jiang, *J. Mater. Chem.*, 2012, **22**, 9494–9496.
- 27 B. Wang, J. Park, D. W. Su, C. Y. Wang, H. Ahn and G. X. Wang, *J. Mater. Chem.*, 2012, **22**, 15750–15756.
- 28 L. Zhang, H. B. Wu and X. W. Lou, *Chem. Commun.*, 2012, **48**, 6912–6914.
- 29 T. Zhu, H. B. Wu, Y. Wang, R. Xu and X. W. Lou, *Adv. Energy Mater.*, 2012, **2**, 1497–1502.
- 30 L. Yu, L. Zhang, H. B. Wu and X. W. Lou, *Angew. Chem., Int. Ed.*, 2014, **53**, 3711–3714.
- 31 J. Q. Dong, D. C. Li, Z. H. Peng and Y. H. Zhou, *J. Solid State Electrochem.*, 2008, **12**, 171–174.
- 32 Q. R. Hu, S. L. Wang, Y. Zhang and W. H. Tang, *J. Alloys Compd.*, 2010, **491**, 707–711.
- 33 W. Luo, Y. Xie, C. Z. Wu and F. Zheng, *Nanotechnology*, 2008, **19**, 075602.
- 34 G. H. Yue, P. X. Yan, X. Y. Fan, M. X. Wang, D. M. Qu, Z. G. Wu, C. Li and D. Yan, *Electrochem. Solid-State Lett.*, 2007, **10**, D29–D31.
- 35 I. Bilecka and M. Niederberger, *Nanoscale*, 2010, **2**, 1358–1374.
- 36 C. Merlet, B. Rotenberg, P. A. Madden, P. L. Taberna, P. Simon, Y. Gogotsi and M. Salanne, *Nat. Mater.*, 2012, **11**, 306–310.
- 37 D. W. Wang, F. Li, M. Liu, G. Q. Lu and H. M. Cheng, *Angew. Chem., Int. Ed.*, 2008, **47**, 373–376.
- 38 Y. S. Hu, Y. G. Guo, W. Sigle, S. Hore, P. Balaya and J. Maier, *Nat. Mater.*, 2006, **5**, 713–717.
- 39 Y. N. Zhou, C. L. Wu, H. Zhang, X. J. Wu and Z. W. Fu, *Electrochim. Acta*, 2007, **52**, 3130–3136.
- 40 Y. J. Kang, H. Chung, C. H. Han and W. Kim, *Nanotechnology*, 2012, **23**, 65401.
- 41 M. D. Stoller and R. S. Ruoff, *Energy Environ. Sci.*, 2010, **3**, 1294–1301.
- 42 N. F. Yu and L. J. Gao, *Electrochem. Commun.*, 2009, **11**, 220–222.

- 43 X. J. He, P. H. Ling, J. S. Qiu, M. X. Yu, X. Y. Zhang, C. Yu and M. D. Zheng, *J. Power Sources*, 2013, **240**, 109–113.
- 44 Z. B. Lei, Z. H. Liu, H. J. Wang, X. X. Sun, L. Lu and X. S. Zhao, *J. Mater. Chem. A*, 2013, **1**, 2313–2321.
- 45 H. W. Wang, Y. L. Wang and X. F. Wang, *New J. Chem.*, 2013, **37**, 869–872.
- 46 H. R. Ghenaatian, M. F. Mousavi and M. S. Rahmanifar, *Electrochim. Acta*, 2012, **78**, 212–222.
- 47 H. C. Gao, F. Xiao, C. B. Ching and H. W. Duan, *ACS Appl. Mater. Interfaces*, 2012, **4**, 2801–2810.